Collinear photothermal deflection spectroscopy with light-scattering samples

Jonathan D. Spear, Richard E. Russo, and Robert J. Silva

An analytical model that incorporates effects of light scattering was developed for dual-beam photothermal deflection spectroscopy. Thermal gradients induced by a modulated excitation beam deflect an optical probe beam which was treated as being of finite dimensions. Mechanisms by which thermal gradients produce refractive index gradients are discussed, with an explicit expression for dn/dT being derived. Experimental studies with suspensions of small latex particles in Nd^{3+} solutions demonstrated that the model accurately predicts both the shape of the deflection signal and the attenuation of the signal due to light scattering. The absolute magnitude of the observed signal is approximately predicted by theory. *Key words:* Photothermal deflection spectroscopy, light scattering.

I. Introduction

Photothermal deflection spectroscopy[1,2] (PDS) is a sensitive method for measuring radiative absorption in transparent and opaque samples. PDS belongs to a class of photothermal spectroscopies which includes photoacoustic,[3] thermal lensing,[4] and interferometric[5] techniques. These methods differ from conventional beam-transmittance spectrophotometry in that they directly monitor temperature fluctuations due to optical radiation absorbed by the sample. In PDS, a probe beam passes through a region of thermal gradients either in a transparent medium adjacent to the sample or within the sample itself. These thermal gradients are accompanied by refractive index gradients which cause the probe beam to be spatially deflected. The amplitude of this deflection is monitored as a measure of radiative absorption. Typically, the focused Gaussian output beam from a He–Ne laser serves as the optical probe, and its deflection is measured by a solid state position sensor.

PDS experiments are generally categorized as being either transverse or collinear. With an opaque solid sample, a transverse arrangement can be used whereby the probe beam propagates through a transparent medium, which is in contact with the surface of the solid. In this case, the excitation beam irradiates the surface at normal incidence and can originate from a pulsed laser, a modulated cw laser, or a modulated tunable lamp. For samples with low levels of radiative absorption, either transverse or collinear arrangements can be used, with the sample itself acting as a medium through which the probe and excitation beams pass. In the transverse arrangement, an excitation beam passes through the sample perpendicularly to the path of a probe beam. The axes of the two beams do not intersect but are slightly offset so that thermal gradients near the overlap region will cause the probe to be deflected radially away from the excitation beam.

In collinear PDS, the two beams are aligned to be nearly parallel and closely overlap within the sample. The geometry of the collinear arrangement is advantageous in that the two beams can interact over a long distance, thereby yielding a greater signal magnitude. With this approach, collinear PDS using a tunable cw excitation laser has been demonstrated to be a sensitive technique for liquid phase analysis of transparent samples and suitable for background correction to compensate for absorption within the solvent.[6] However, to the best of our knowledge, there has been no published work regarding the effects of light scattering in collinear PDS. Light scattering is important because it can influence the measurement of environmental samples, which usually contain particulates. For this reason, we investigated collinear PDS with a modulated cw dye laser, using samples whose light scattering coefficients significantly exceeded their optical absorption coefficients. An important goal of this work was to develop an understanding of how light scattering in a partially transparent sample influences the observed PDS signal.

Theoretical models for collinear PDS using a modulated cw source were described initially by Jackson *et*

Robert J. Silva is with the Lawrence Livermore National Laboratory, Livermore, California 94550; the other authors are with the Lawrence Berkeley Laboratory, Berkeley, California 94720.

Received 24 October 1989.
0003-6935/90/284225-10$02.00/0.

al.[1] and subsequently by Vyas *et al.*,[7] who expanded the model to incorporate measurements made in a flowing sample. These studies are fairly rigorous in their treatment of the thermal gradients produced within the medium. However, in both models, the probe beam was idealized to behave as an infinitesimally thin ray. This simplified treatment of the probe beam becomes inaccurate in situations where the probe beam radius is comparable to the thermal diffusion length or to the excitation beam radius, and in many cases all three of these dimensions are comparable. For example, at a modulation frequency of $\omega/2\pi = 50$ Hz, the thermal diffusion length in water is 30 μm. Therefore, it is necessary to develop a more detailed analysis that accounts for the finite size of the probe beam. One method is to treat the probe beam as Gaussian and solve the appropriate equations for wave propagation through the medium. This approach has been taken by Mandelis and Royce[8] for the special case involving 1-D chemical diffusion near an electrode surface. Another method, which has been successfully applied in the analysis of transverse PDS experiments,[9–11] is to treat the probe beam as a cluster of ray segments. In this analysis, the contribution from each ray segment to the overall deflection of the probe beam is weighted by the probe beam intensity and integrated over the entire volume through which the probe beam passes. We applied this ray segment method to collinear PDS and incorporated light scattering as a parameter within the model. The physical principles on which our model is based are heating of the sample by optical absorption, thermal diffusion in the medium, temperature dependence of refractive index, and refraction of optical rays. These processes are the same as those considered by previous authors. Our work significantly differs from previous works in that we report the absolute deflection of the probe beam in real units of radians rather than arbitrary units.

II. Theoretical

A. Simplified Example

To describe qualitatively the effects of light scattering, let us first consider a simple collinear PDS experiment as in Fig. 1, in which the excitation and probe beams are perfectly collimated and parallel to each other. The beams travel through a sample of thickness Z (cm). If the excitation beam is modulated, the thermal diffusion length in the sample is defined as $\sqrt{\alpha_{th}/\pi f}$ (cm), where α_{th} is the thermal diffusivity of the sample (cm^2/s), and f is the modulation frequency (Hz). We initially assume that the diameters of the beams and the thermal diffusion length in the sample are much smaller than the sample thickness. As the excitation beam passes through the sample, its optical power is reduced exponentially with an extinction coefficient equal to the sum of its scattering coefficient α_s (cm^{-1}) and absorption coefficient α_a (cm^{-1}). For weakly absorbing samples, α_a generally is $\ll Z^{-1}$, but our treatment will allow α_s to be of comparable magnitude. Therefore, any significant extinction of the excitation beam is due to scattering rather than absorption. When a photon from the excitation beam is scattered, it may be subsequently absorbed in a different region of the sample. Typically, this happens after the photon has traveled a distance of the order of $1/\alpha_a$ away from its original path. Because this dimension greatly exceeds the beam diameters, the subsequent absorption is unlikely to occur near a region through which the probe beam passes. Therefore, scattered excitation radiation does not contribute appreciably to photothermal deflection of the probe beam. However, the attenuation of the excitation beam due to scattering exponentially reduces the power available for producing thermal gradients in the sample, thereby causing a decrease in the amplitude of the observed deflection signal. This effect can be described via a clarity factor (C.F.), which we define as the ratio of the observed deflection amplitude in the presence of scattering to the deflection amplitude that would be observed without scattering. The magnitude of the thermal gradients produced at any point along the z-axis is proportional to the available power from the excitation beam. Therefore, the overall measured deflection of the probe beam is proportional to an integral over the z-axis of the excitation beam power. Let us define P_0 as the available power incident on the sample at $z = 0$. The clarity factor can be computed simply by comparing the integrals of the available power along the z-axis for the two cases:

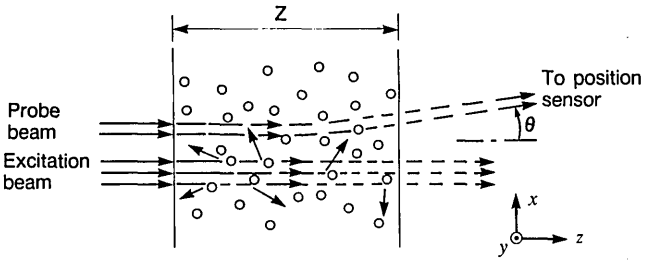

Fig. 1. Simplified 2-D geometry for the collinear PDS experiment in the presence of light scattering.

$$\text{C.F.} = \frac{\int_0^Z P_0 \exp(-\alpha_s z)dz}{\int_0^Z P_0 dz} = \frac{[1 - \exp(-\alpha_s Z)]}{\alpha_s Z}. \quad (1)$$

This expression describes the decrease in PDS signal amplitude that is attributable to scattering. Therefore, if PDS is used to measure the absorption coefficient of a material that has a known or measurable scattering coefficient at the excitation beam wavelength, the measured value must be adjusted by this factor. The above formula is accurate only for collinear PDS systems whose geometries closely approximate the simplifications of this example.

The optical probe beam also is scattered in the sample, so that the spot projected by the probe beam onto the position sensor is diminished in intensity. Because the angular extent of the position sensor is small, we approximate that no scattered photons are measured by the detector. We also note that the position

measurement is independent of beam intensity. Therefore, it is permissible in our analysis to ignore the attenuation of the probe beam. However, practical considerations in the experiment dictate that a significant portion of the probe beam be able to reach the plane of the detector, so that the device can still measure the position of the spot. This places a restriction on the type of scattering sample that can be measured by collinear PDS: the sample must be optically uniform on the scale of the beam diameters. In other words, light scattering particulates should have an effective cross section that is much smaller than the cross section of the beams. Otherwise, a single particulate could obstruct the paths of the beams, thereby disrupting the PDS signal.

B. More Complex Geometry

The geometrically simple model described above is useful for understanding qualitative effects caused by light scattering, but the idealizations made for this special case do not generally apply to all collinear PDS systems. For a practical arrangement, the two beams are focused to such an extent that their diameters vary significantly as the beams propagate through the sample. Also, the experiment may be arranged so that the beams overlap within the sample at a finite angle. A motivation for such a design is to reduce unwanted photothermal deflection effects that might occur at windows and other optical elements and to avoid the possibility of having optical radiation from the excitation beam reach the position sensor. These geometric conditions affect the way in which the excitation beam produces thermal gradients along the z-axis and also the way in which the probe beam is deflected by these thermal gradients. Therefore, it becomes necessary to perform a more detailed analysis that account for these parameters. Our approach for incorporating these effects is to determine the induced thermal gradients, use this information to deduce refractive index gradients, and then perform a weighted integration over the entire volume through which the probe beam passes.

Figure 2 is a diagram of a typical collinear PDS arrangement. We define our coordinate system as follows: The probe beam propagates along the z-axis, entering the sample at the origin. The probe beam is Gaussian and has a $(1/e^2)$ waist radius w_{0p}, which is located at point $(0,0,z_{0p})$. The excitation beam also is Gaussian and has a $(1/e^2)$ waist radius w_0 located at point (x_0,y_0,z_0). This excitation beam propagates in a direction parallel to the y-z plane and intersects the x-z plane at an angle ϕ. x_0 defines the distance of the closest approach between the propagation axes of the two beams. The beams are offset in the horizontal direction by this amount, and the position sensor measures the horizontal deflection of the probe beam.

C. Thermal Gradients

If we assume that heat transfer within the sample occurs by conduction, the transient distribution of

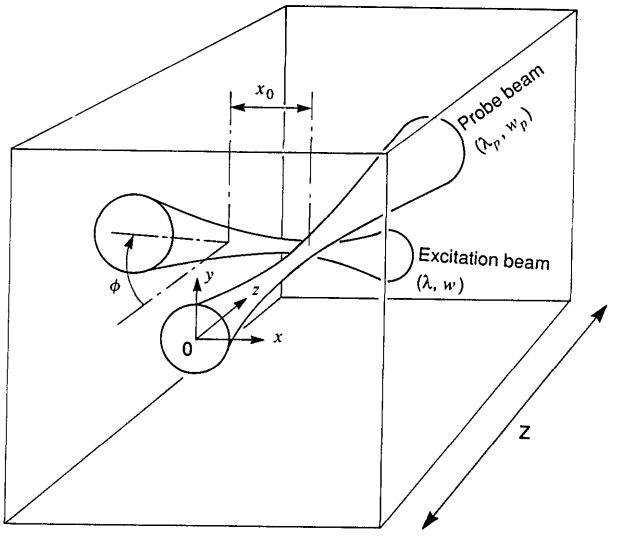

Fig. 2. More detailed 3-D geometry in a useful collinear PDS experiment. The model must account for changing beam diameters and finite overlap angle ϕ.

temperature T in the sample obeys the thermal diffusion equation

$$\nabla^2 T - \frac{1}{\alpha_{\text{th}}}\frac{dT}{dt} = \frac{-Q(x,y,z,t)}{\kappa}, \tag{2}$$

where κ is the thermal conductivity (W/cm K), α_{th} is the thermal diffusivity (cm^2/s), and Q is the volumetric heating rate (W/cm^3) caused by absorption of the excitation beam. Thermal models for PDS reported in the literature[1,7] have investigated the case in which Q is sinusoidally modulated. We consider a different situation in which Q is modulated as a square wave with 50% duty cycle and frequency f. This model accurately represents a cw laser beam passing through a mechanical chopper-wheel. By approximating that ϕ is small, we can write

$$Q = \frac{2\alpha_a P_0 \exp(-\alpha_s Z)}{\pi w^2}\left[\exp\left(\frac{-2r^2}{w^2}\right)\right] \quad \text{for } j/f \le t \le \left(j+\frac{1}{2}\right)\Big/f,$$

$$Q = 0 \quad \text{for } t < 0, \left(j+\frac{1}{2}\right)\Big/f < t < (j+1)/f, \tag{3}$$

for all whole numbers j {0,1,2,. . .}. For small values of ϕ, $r = \sqrt{(x-x_0)^2 + [y + (z-z_0)\tan\phi - y_0]^2}$ is the radial distance measured from the propagation axis of the excitation beam. w is the $(1/e^2)$ beam radius, which is given by the equation of propagation for a Gaussian beam:

$$w^2 = w_0^2\left\{1 + \left[\frac{\lambda(z-z_0)}{\pi w_0^2 n}\right]^2\right\}, \tag{4}$$

where λ is the wavelength in vacuum of the excitation light, and n is the refractive index of the sample. The intensity of the excitation beam varies much more in the radial direction than it does along the axis of propagation. For this reason, we can approximate that thermal gradients exist in the radial direction but are not significant along the z-axis. Therefore, Eq. (2)

reduces to a 1-D problem in r. For PDS, we are interested not in the temperature itself but in dT/dr, the gradient of the temperature. We can make use of the result given by Jackson *et al.*,[1] who solved a similar problem for the case of a sample heated by a single square pulse. If the heating function of Eq. (3) were to be restricted so that it was applied only during the first square pulse ($0 \le t \le 1/2f$), the solution for the thermal gradients would be given by

$$\frac{dT}{dr} = \frac{\alpha_a P_0 \exp(-\alpha_s Z)}{2\pi r\kappa}\left[\exp\left(\frac{-2r^2}{w^2}\right) - \exp\left(\frac{-2r^2}{w^2 + 8\alpha_{th}t}\right)\right] \qquad 0 \le t \le 1/2f,$$

$$\frac{dT}{dr} = \frac{\alpha_a P_0 \exp(-\alpha_s Z)}{2\pi r\kappa}\left[\exp\left(\frac{-2r^2}{w^2 + 8\alpha_{th}(t - 1/2f)}\right) - \exp\left(\frac{-2r^2}{w^2 + 8\alpha_{th}t}\right)\right] \qquad t \ge 1/2f. \quad (5)$$

Now, because the square-wave modulation function in Eq. (3) can be viewed as a sum of square pulses, each separated by a period f^{-1}, we can apply the superposition principle to individual solutions for single square pulses. The resulting solution to Eqs. (2) and (3) can then be expressed compactly in summation form:

$$\frac{dT}{dr} = \sum_{j=0}^{N} \frac{\alpha_a P_0 \exp(-\alpha_s Z)}{2\pi r\kappa}(-1)^j\left\{\exp\left(\frac{-2r^2}{w^2}\right) - \exp\left[\frac{-2r^2}{w^2 + 8\alpha_{th}(t - j/2f)}\right]\right\} \qquad t \ge 0, \quad (6)$$

where N is the greatest whole number so that $N \le (2ft)$. Each value of j in the summation corresponds to a previous point in time at which the excitation beam was turned on or off by the mechanical chopper. Because of the $(-1)^j$ factor, the first exponential term within the brackets will alternately cancel itself out of the summation, depending on the parity of N.

D. Refractive Index Gradients

In both PDS and thermal lensing experiments, it is common practice to link refractive index gradients directly to thermal gradients:

$$\nabla n = \nabla T \frac{dn}{dT}, \quad (7)$$

where dn/dT, the temperature coefficient of the refractive index, is considered to be an inherent material parameter of the medium through which the probe beam passes. In the literature on PDS, little attention has been paid to the mechanisms which contribute to this important property, and numerical values for this property have not been extensively measured for many materials. In the following section we derive an explicit expression for dn/dT in terms of material parameters that are well known.

There are two types of mechanisms that can contribute to dn/dT. One involves thermal expansion of the medium and can be described with the assumption that the individual molecular or electronic polarizabilities within the material remain constant. The other mechanism is related to thermal shifts in the absorption bands of the medium. If the nature of these thermal changes is known in detail, the change in the refractive index of the material can be determined via the Kramers-Kronig dispersion relations. The wavelength of the optical probe beam used in PDS usually is chosen so that it does not coincide with any strong absorption bands of the material. Therefore, this second type of mechanism is negligible, and dn/dT can be attributed exclusively to expansion of the medium. For this reason, the Lorentz-Lorenz relation holds:

$$\frac{1}{\rho}\left(\frac{n^2 - 1}{n^2 + 2}\right) = \text{constant}, \quad (8)$$

where ρ is the density of the medium. Now we implicitly differentiate this expression with respect to temperature. After algebraic simplification, one obtains the following equation:

$$-\frac{1}{\rho}\frac{d\rho}{dT}(n^2 - 1) + \frac{6n}{(n^2 + 2)}\frac{dn}{dT} = 0. \quad (9)$$

If the material is a solid, localized mechanical stresses will be produced by the thermal gradients, and a calculation of thermal expansion requires information regarding the boundary conditions of the particular experiment. This implies that, for the purposes of photothermal spectroscopies, dn/dT is not strictly an inherent material parameter of solids. To determine an effective value of dn/dT for a solid material that is inhomogeneously heated as in PDS, it would be necessary to solve thermoelastic strain equations,[12] using the specific parameters and boundary conditions of the individual experiment.

Fortunately, for most PDS experiments, the medium through which the probe beam passes will be either a gas or a liquid, free to expand with no resulting thermal stresses. Because this is true, one can make use of the fact that $\beta = -(1/\rho)(d\rho/dT)$ is the commonly measured thermal expansion coefficient (volumetric) of the fluid material and rearrange Eq. (9) to obtain

$$\frac{dn}{dT} = -\frac{\beta}{6n}(n^2 - 1)(n^2 + 2). \quad (10)$$

Our derivation provides a physical explanation for why dn/dT should be linearly proportional to the thermal expansion coefficient.[13] Equation (10) expresses dn/dT in terms of two physical quantities whose values are commonly measured and recorded. This material parameter is important, not only for photothermal spectroscopies but also for related topics such as thermal self-focusing of laser beams.[14] Therefore, the equation can be used to estimate dn/dT for a particular material without the need for an actual experimental measurement. Table I compares published experimental data for dn/dT for water and some organic liquids to those values that are predicted by Eq. (10). Agreement is generally good, with the two values differing typically by <15%. It is interesting to note that for gases, where n is close to unity and the ideal gas law gives $\beta = T^{-1}$, Eq. (10) simplifies to

$$\frac{dn}{dT} \approx \frac{-(n - 1)}{T}. \quad (11)$$

Table I. Comparison of Experimental Values for dn/dT with Those Given by Eq. (10); Sources for Data are in Parentheses

Compound	$10^3\,\beta$ (°C^{-1})	n	$10^4\,dn/dT$ Experimental (°C^{-1})	$10^4\,dn/dT$ from Eq. (10) (°C^{-1})
Acetone	1.487 (15)	1.355 (17,18)	−5.0 (17,18)	−5.87
Benzene	1.237 (15)	1.495 (17,18)	−6.4 (17,18)	−7.21
CCl_4	1.236 (15)	1.454 (17,18)	−5.8 (17,18)	−6.49
CS_2	1.218 (15)	1.617 (17,18)	−7.7 (17,18)	−9.35
Ethanol	1.12 (15)	1.358 (17,18)	−3.9 (17,18)	−4.46
Methanol	1.199 (15)	1.325 (17,18)	−3.9 (17,18)	−4.28
Pentane	1.608 (15)	1.353 (17,18)	−5.5 (17,18)	−6.30
Water, $T = 20$°C	0.2066 (16)	1.331 (19)	−0.877 (19)	−0.753
Water, $T = 25$°C	0.2571 (16)	1.331 (19)	−1.038 (19)	−0.937
Water, $T = 30$°C	0.3031 (16)	1.331 (19)	−1.184 (19)	−1.104

This expression is consistent with the empirical formula used by Murphy and Aamodt[20] and is further evidence of the general applicability of Eq. (10) to thermally expansive fluids.

E. Deflection of the Probe Beam

Now that the refractive index gradients can be obtained explicitly, an expression can be derived for predicting the deflection of the probe beam. As previously mentioned, it is not necessary to account for attenuation of the probe beam due to absorption or scattering. Because the position sensor measures the intensity weighted average displacement of the probe beam spot, this deflection calculation is fairly straightforward. The deflection (in radians) of a single ray of light, passing through a medium with small refractive index gradients perpendicular to the direction of propagation, is given by

$$\theta = \int_0^Z \frac{\nabla n}{n}\,dz. \tag{12}$$

The Gaussian probe beam of finite dimensions can be analyzed by dividing it into cross-sectional slices along the z-axis. Every section can then be viewed as a cluster of short ray segments arranged so that the density of ray segments is proportional to the optical intensity. Each ray segment is deflected by a different amount, depending on the refractive index gradient at that location. The mean rate at which one of these ray segments is deflected, $d\theta/dz$ (rad/cm), can be computed by an intensity weighted integral over the entire x-y plane:

$$\frac{d\theta}{dz} = \frac{\int_{-\infty}^{\infty} dx \int_{-\infty}^{\infty} I_p \frac{\nabla n}{n}\,dy}{\int_{-\infty}^{\infty} dx \int_{-\infty}^{\infty} I_p\,dy}, \tag{13}$$

where I_p is the intensity of the probe beam, which has a Gaussian proportionality: $I_p \propto \exp[-2(x^2 + y^2)/w_p^2]$. The probe beam radius w_p behaves in a similar fashion to the excitation beam radius, as in Eq. (4). Accordingly, we can write

$$w_p^2 = w_{0p}^2\left\{1 + \left[\frac{\lambda_p(z - z_{0p})}{\pi w_{0p}^2 n}\right]^2\right\}. \tag{14}$$

Now, as for the single ray, we can integrate Eq. (13) over the z-axis to obtain an expression for the intensity weighted average deflection of a ray at the exiting boundary of the sample material:

$$\theta = \int_0^Z dz \int_{-\infty}^{\infty} dy \int_{-\infty}^{\infty} \frac{2\exp[-2(x^2 + y^2)/w_p^2]\nabla n}{w_p^2 \pi n}\,dx. \tag{15}$$

This expression, along with Eqs. (6), (7), (10), and (14), describes the evolution of the measured PDS signal in time. Note that the position detector is usually placed in air (where $n \approx 1$) at some distance from the sample. For this reason, to determine the actual deflection angle measured by the detector, one should apply Snell's law of refraction to the rear plane of the sample, and the n term drops out of the denominator.

III. Numerical Computation

A. Simulated Alignment

The numerical calculation of the volumetric integral in Eq. (15) is fairly straightforward. To reduce the number of necessary integrand evaluations, we constrain the integrations over the x- and y-axes to cover only the ranges from $-2w$ to $+2w$. Because a square cross section of a Gaussian beam with these dimensions includes more than 99.98% of its power, this approximation is reasonable. We compute the integral by dividing the volume first into cross sections along the z-axis. Then each of the cross sections is separated into a grid of rectangles. The integrand is evaluated at the center of each rectangular element and summed over all the elements. Because the integrand is a well behaved function, we find that more complicated methods are not needed and that the calculated value usually converges to within 1% of its limit value when 512 evaluations are made (eight along each of the three axes). It is interesting to note that the task of numerical computation has been simplified by the fact that an analytical solution could be obtained for the thermal gradients in this case of square-wave modulated cw PDS. This holds true also for the case of pulsed PDS. However, for the case of sinusoidally modulated cw PDS, the solution for thermal gradients must be expressed in integral form,[1] and the computation becomes more difficult.

To test our model, a numerical simulation of the evolution of the deflection signal was performed with parameters that could later be duplicated experimentally. The beam waist radii, w_0 and w_{0p}, were each set at 25 μm. The wavelengths of the probe and excitation beams were 632.8 and 575 nm, respectively. The beam waists were initially located at $z = 0.5$ cm with $y_0 = 0$. The path length of the sample Z was 1 cm. The overlap angle ϕ was 0.5°, and the modulation frequency was 47 Hz. The sample was a dilute aqueous solution; thus the following material parameters for water[16] were used: $\kappa = 5.99 \times 10^{-3}$ W/cm K and $\alpha_{th} = 1.43 \times 10^{-3}$ cm^2/s. For an ambient temperature of $T =$

24°C, the values of $n = 1.331$ and $dn/dT = -1.0 \times 10^{-4}$ K^{-1} were used (from Table I). P_0 was 40 mW and α_a was 9×10^{-3} cm^{-1}, which corresponds to the absorption coefficient at 575 nm of a 1.3×10^{-3}-M solution of Nd^{3+}. Initially, the scattering coefficient α_s was set to be zero.

In an experimental situation, it is difficult and often unnecessary to measure the actual value of x_0 precisely. In practice, one can fix the path of the probe beam and then carefully adjust the relative position of the excitation beam until a maximum deflection signal in the x-direction is observed. We numerically imitated this physical procedure by using our computation routine to vary this geometric parameter. The result of a numerical simulation is displayed in Fig. 3, which shows the evolution of the PDS signal beginning when the excitation beam is turned on at $t = 0$. Initially, there is a periodic deflection of the probe beam (the ac signal), which is synchronous with the modulation of the excitation beam. This ac deflection is accompanied by a more slowly developing dc deflection, which reaches a steady state after several periods. After this steady state level has been reached, the dc signal can be ignored, and the periodic waveforms that are produced can be analyzed. When we varied the x_0 parameter in our simulation, we found that the waveform had a maximum peak-to-peak value of 122 μrad when $x_0 = \pm 28$ μm (Fig. 4).

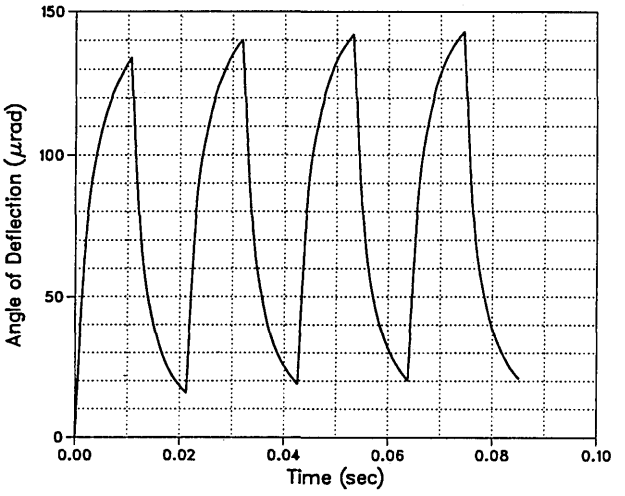

Fig. 3. Simulated deflection signal for beam offset $x_0 = -28$ μm. Other parameters are described in the text.

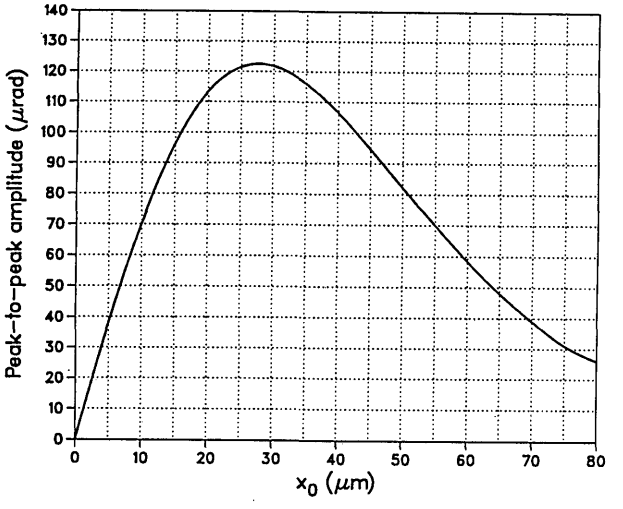

Fig. 4. Simulated peak-to-peak amplitude of deflection signal vs beam offset x_0. The beam waist radius w_{0p} was set at 50 μm.

B. Effects of Probe Beam Size

Selecting an appropriate probe beam size is an important consideration for the design of a PDS system. For this reason, we used our model to simulate how changes in the probe beam radius affect the amplitude of the deflection signal. In general, a tightly focused beam can be directed to pass completely through a region where refractive index gradients are at a maximum, thereby enabling a large signal magnitude to be obtained. This might lead one to think that the probe beam should be focused as small as possible. However, as can be determined from Eq. (14), a Gaussian beam with a small waist has a large far field divergence angle. If the probe beam diverges to a size greater than that of the position sensor, measurement of the beam's deflection can become difficult. Another practical limitation is that, if inhomogeneities such as particulates exist in the sample and are of a size comparable with that of the probe beam, the noise or error due to these inhomogeneities is likely to be increased as the probe beam radius is decreased.

To check whether our choice of 25 μm is appropriate for the beam waist radius w_{0p}, we performed another set of numerical simulations, varying w_{0p} from 2.5 to 100 μm. For each value of w_{0p}, x_0, the beam offset was adjusted slightly until a maximum deflection amplitude was obtained. All other geometric and material parameters were maintained as before. Figure 5 gives the results of these numerical simulations, showing the peak-to-peak amplitude as a function of the probe beam waist radius. The maximum amplitude can be obtained when w_{0p} is set at $\sim$17 μm. If the waist radius

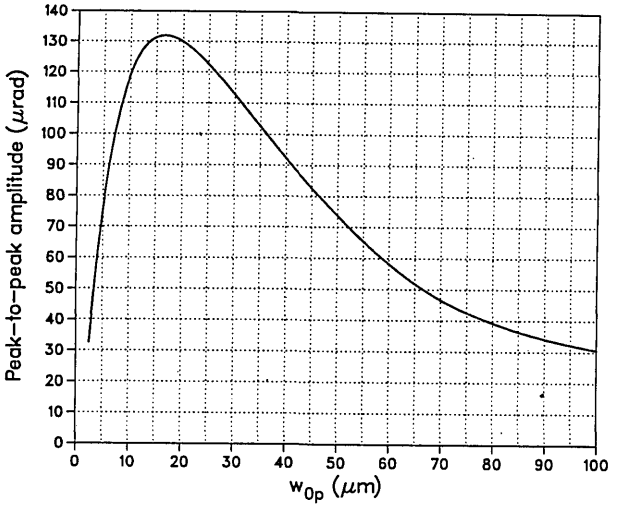

Fig. 5. Simulated peak-to-peak amplitude of the deflection signal vs probe beam waist radius w_{0p}. For each value of w_{0p}, the beam offset x_0 was optimized for the maximum signal amplitude.

is reduced below this point, the divergence of the beam within the sample causes the signal amplitude to be diminished. Because the amplitude obtainable from a 25-μm waist radius is close to the peak of the curve, this choice of w_{0p} is justified. We also performed a simulation using the simplified assumption that the probe beam propagates as a single infinitesimally thin ray, not limited by diffraction effects. For this case, our simulation gave that the peak-to-peak amplitude was 171 μm and occurred when x_0 was set at ± 21 μm.

C. Simulated Scattering Effects

Once the alignment of the system has been optimized for maximum deflection amplitude, it is possible to investigate the effects of light scattering on the deflection signal by adjusting the light scattering parameter. We varied the value of α_s from 0 to 4 cm^{-1}, maintaining the geometric parameters that were determined above. These parameters correspond to the symmetric case in which the beams are centrally focused in the sample. We were also interested in observing light scattering effects for cases in which the beams would be either prefocused or postfocused within the sample. For examples, we selected z_0 and z_{0p} to be equal both to 0.2 cm (prefocused case) and then to 0.8 cm (postfocused case). For each case, α_s was initially set to 0, and then a simulated alignment of the system was performed by maximizing the peak-to-peak deflection as a function of x_0 and y_0. The optional value for x_0 was found to be ± 29 μm for both cases. The optimal value for y_0 was -24 μm for the prefocused case and $+24$ μm for the postfocused case. Our simulation showed that, in the absence of light scattering, the peak-to-peak amplitude of the resulting deflection signal was only 4% lower for these two cases than for the centrally focused case. Using our numerical simulation, we observed an expected decrease in the peak-to-peak amplitude of the periodic deflection signal, from which the clarity factor was calculated. These data are shown in Fig. 6 for each of the three beam waist locations along the z-axis. Note that the extent to which light scattering decreases the PDS signal is highly dependent on the positioning of the beam waists along the z-axis. Therefore, a precise determination of the focusing state of the beams is necessary for one to be able to account properly for light scattering effects. The signal attenuation effect can be minimized by prefocusing the beams within the sample. This trend occurs because the beams interact most strongly when their diameters are small, and for the prefocused case this region occurs before scattering attenuates the excitation beam. Postfocusing in the presence of high scattering causes the undesirable effect of greatly reducing the measured deflection signal.

IV. Experimental

Figure 7 is a diagram of the apparatus that was used for our experimental work. A Spectra-Physics model 171 argon-ion laser and a tunable Coherent model CR-599 dye layer with rhodamine 560 dye provided the excitation radiation. The dye laser beam was modu-

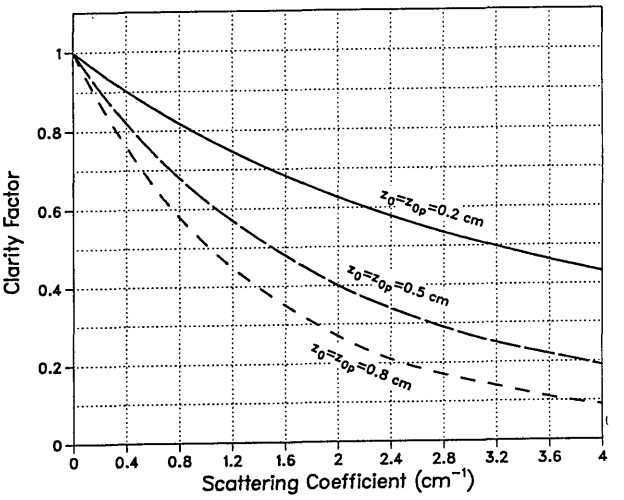

Fig. 6. Computed values for the clarity factor vs scattering coefficient α_s for three different focusing states of the optical beams: $z_0 = z_{0p} = 0.2$ cm (solid line); $z_0 = z_{0p} = 0.5$ cm (broken line); $z_0 = z_{0p} = 0.8$ cm (dashed line).

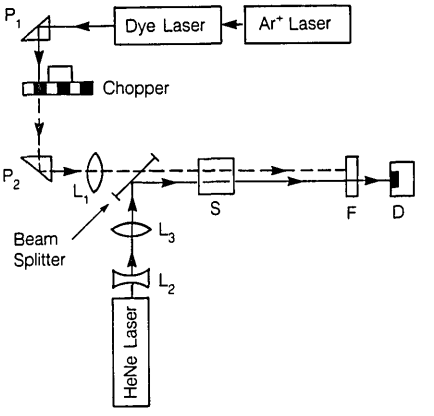

Fig. 7. Schematic diagram of the apparatus used for collinear PDS experiments.

lated by a mechanical chopper, and its path was folded by two prisms, P_1 and P_2. These prisms were mounted onto dual axis tilt plates to allow for fine adjustment of the beam position and angle within the sample. A He–Ne laser (Uniphase model 1303P) served as the source of the probe beam. The two beams were incident on opposite sides of a dielectric beam splitter. The transmitted portion of the excitation beam and the reflected portion of the probe beam overlapped within a quartz sample cuvette at point S. The cuvette contained the aqueous sample mixtures within a 1-cm optical path. The excitation beam was focused by a lens L_1 with a focal length of 10 cm. The probe beam was first expanded by a concave lens L_2 with a focal length of -5 cm, then focused by a convex lens L_3 with a focal length of 6.3 cm. The separation between these two lenses was 9.4 cm. This lens arrangement focused both beams to the waist radii of 25 μm that were quoted in the previous section. These dimensions were measured with a photodiode mounted behind a movable pinhole to an accuracy of ± 5 μm. The waists were

located in the center of the sample cell, at $z = 0.5$ cm. The accuracy of this measurement was approximately ±0.05 cm. The mechanical chopper was operated at 47 Hz, as mentioned in the previous section. The excitation beam was directed so that it overlapped the probe beam at 0.5°. The position sensor D was a continuous, single axis, dual cathode photodetector (UDT model LSC-5D), which was placed at a distance of 17 cm from the sample cell and connected to a UDT model 301-DIV amplifier. We observed that the electrical output of this detector–amplifier combination changed by 0.25 V when the optical spot was linearly translated by 100 μm. From this test, we were able to measure the absolute values of our observed deflection signal using 425 V/rad as the calibration constant. A narrow bandpass optical filter F rejected stray light from the excitation beam and allowed only the light from the probe beam to reach the detector.

The excitation beam wavelength was tuned to 575 nm, and a sample solution of 1.3×10^{-3}-M Nd^{3+} in 4×10^{-3}-M HCl was placed in the cuvette. Neodymium was selected because its absorption peak at 575 nm overlaps the available tuning range of the dye laser. A small amount of surfactant (1 part in 200 by volume of Kodak Photoflo 200) was then added to the mixture. The inclusion of this surfactant was necessary for subsequent tests involving light-scattering latex spheres and did not noticeably affect the deflection signal. The beam deflection was monitored with a Tektronix model 7854 storage oscilloscope. Fine positioning adjustments were made on the excitation beam until the oscilloscope trace displayed a maximum peak-to-peak deflection. To record the transient deflection signal from the moment the excitation beam was turned on, at $t = 0$, the shutter from a 35-mm camera was placed in the path of the excitation beam. When the camera shutter was opened, the camera trigger normally intended for an electronic flash attachment was used to trigger the oscilloscope. A photograph of this oscilloscope trace is shown in Fig. 8. The shape of this waveform compares favorably with the corresponding simulated waveform of Fig. 3. The peak-to-peak amplitude of the observed deflection signal, as taken from the oscilloscope trace, is 210 μrad. This value is greater than the 122-μrad amplitude that is predicted by the theoretical model. We are unsure of the cause of this discrepancy. Perhaps it is due to an accumulation of measurement errors, incorrect material parameters, or some limitation of the theory. In any case, the discrepancy in the absolute amplitude does not prevent us from obtaining and comparing normalized absorption spectra of aqueous samples.

To induce light scattering, latex spheres (Duke Scientific Catalog 5008A, diameter = 0.087 μm) were mixed into the sample solution. These spheres remain in colloidal suspension because they carry a mildly negative electrical surface charge, which causes them to repel each other. We found that when the spheres were added to a solution of Nd^{3+} ions, the spheres would visibly flock together. The reason for this was that the positively charged Nd^{3+} ions acted as electronic bridges between individual spheres. Adding a surfactant helped to prevent the spheres from flocking. All liquid mixtures observed in this study contained equal amounts of Nd^{3+}, HCl, and surfactant, with varying concentrations of latex spheres. Because the diameters of the latex spheres are much less than the wavelength of optical radiation, they behave approximately as Rayleigh scatterers. The scattering coefficient α_s was measured by passing the laser beams through the solution and using a photodiode to measure the power of the unscattered transmitted beams. Comparisons between the excitation beam and probe beam showed that α_s was approximately proportional to λ^{-4}, as expected from Rayleigh theory. The scattering coefficients of the mixtures that we produced varied between 0 and 3.8 cm^{-1} at the excitation wavelength. To ensure that the spheres did not contribute to the absorption coefficient of the sample or affect the signal in any way other than by scattering, the wavelength of the excitation beam was scanned over the absorption peak of Nd^{3+}. An absorption spectrum for each mixture was obtained by sending the deflection signal into an EG&G Ortec model Ortholoc-SC 9505 lock-in amplifier, which used the timing signal from the mechanical chopper as a frequency reference. The lock-in amplifier phase was adjusted to provide maximum signal amplitude. A silicon photodiode monitored a portion of the unmodulated output of the dye laser, and a Stanford Research Systems model SR235 analog processor divided the output of the lock-in by the amplified photodiode signal to provide for normalization of the data. The wavelength of the dye laser was scanned at a constant speed from 565 to 580 nm, and the normalized deflection signal was traced on an X-Y plotter.

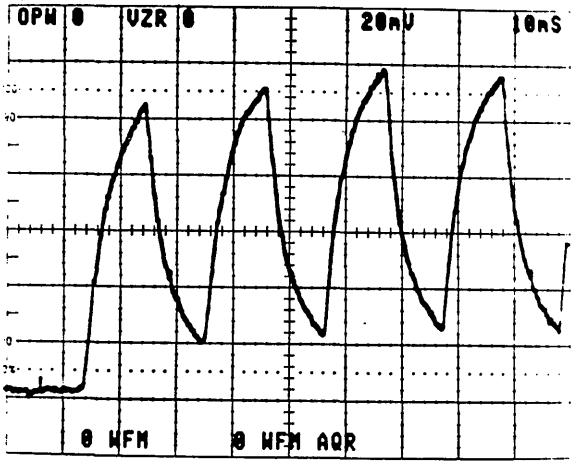

Fig. 8. Oscilloscope trace of observed deflection signal. The vertical scale units are 4.7×10^{-5} rad/div. Horizontal units are 10 ms/div.

Figure 9 shows the absorption spectra that were obtained for three of the sample mixtures. Because the peak-to-peak deflection amplitude is normalized with respect to the excitation beam power P_0, the vertical scale units are given as (μrad/mW). The attenuation effect due to light scattering can be seen as a decrease in the height of the recorded absorption peak.

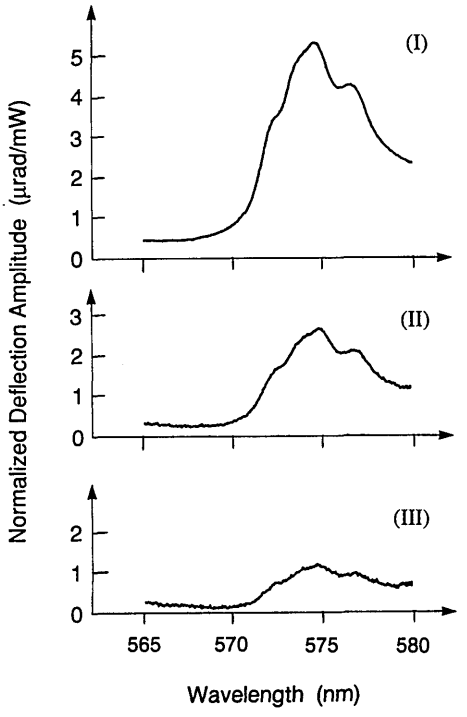

Fig. 9. Photothermal deflection spectra for three samples with different scattering coefficients: $\alpha_s = 0$ (I); $\alpha_s = 1.6\ \text{cm}^{-1}$ (II); $\alpha_s = 2.9\ \text{cm}^{-1}$ (III). Beams are focused in the middle of the sample cell ($z_0 = z_{0p} = 0.5$ cm). The peak-to-peak amplitude (μrad) is normalized with respect to P_0, the excitation power (mW) entering the sample.

As the scattering coefficient was increased, the shape of the recorded spectrum remained essentially constant, and the experimental noise was increased only slightly. This noise increase can be attributed to shot noise in the position detector, which is inversely proportional to the intensity of the probe beam. When the scattering coefficient at the excitation wavelength is 3 cm^{-1}, only 13% of the probe beam light flux is transmitted to the detector. The scattering coefficients observed in these experiments are quite high and probably exceed those that would be encountered in realistic environmental samples. It is remarkable that collinear PDS can be used successfully to obtain spectra of samples whose scattering coefficients are more than 2 orders of magnitude greater than their absorption coefficients, as this type of spectral analysis would not be possible by conventional beam transmittance spectrophotometry.

For each spectrum of a light scattering sample, we measured the vertical distance between the Nd^{3+} absorption peak, near $\lambda = 575$ nm, and the lowest point of the curve, near $\lambda = 568$ nm. Clarity factors were obtained by comparing this distance with the corresponding distance on the spectrum taken for the sample that had no light scattering. Data for these clarity factors are shown in Fig. 10 along with the theoretically predicted values. Agreement is good, showing that the clarity factor developed in the theoretical model can be applied to observed photothermal deflection spectra, to deduce true absorption coefficients of light scattering samples.

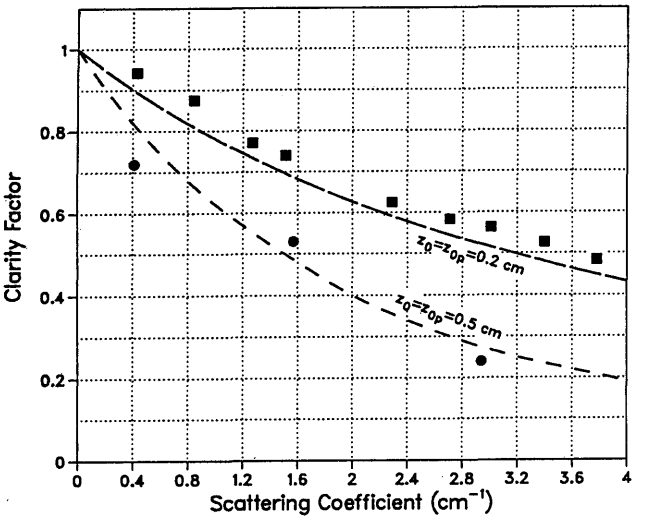

Fig. 10. Clarity factor vs scattering coefficient α_s taken from normalized spectra for $z_0 = z_{0p} = 0.2$ cm (square data points) and $z_0 = z_{0p} = 0.5$ cm (circular data points). Theoretical curves from Fig. 6 are repeated for comparison.

IV. Summary

We have developed a 3-D theoretical model for collinear PDS based on thermal conduction and the finite sizes of both the probe and excitation beams. This model is accurate in describing the form of the deflection signal but only approximates its absolute magnitude. Also, we have derived an equation which relates dn/dT of transparent fluids to more commonly measured material parameters. When light scattering causes a significant portion of the excitation beam to be extinguished, the observed deflection signal is reduced by a predictable factor. This effect can be minimized by focusing the beams toward the front rather than the center of the sample. Experiments demonstrate that, when the scattering particulates are small, collinear PDS can be performed in highly scattering samples. Scattering of the probe beam radiation can be ignored as long as the sample remains transparent to a portion of the probe beam.

This work was performed under the Lawrence Livermore National Laboratory contract W-7405-ENG-48 for the U.S. Department of Energy.

References

1. W. B. Jackson, N. M. Amer, A. C. Boccara, and D. Fournier, "Photothermal Deflection Spectroscopy and Detection," Appl. Opt. **20**, 1333–1344 (1981).
2. A. C. Boccara, D. Fournier, and J. Badoz, "Thermo-Optical Spectroscopy: Detection by the Mirage Effect," Appl. Phys. Lett. **36**, 130–132 (1980).
3. A. C. Tam, "Applications of Photoacoustic Sensing Techniques," Rev. Mod. Phys. **58**, 381–431 (1986).
4. H. L. Fang and R. L. Swafford, "The Thermal Lens in Absorption Spectroscopy," in *Ultrasensitive Laser Spectroscopy*, D. S. Kliger, Ed. (Academic, New York, 1983), Chap. 3, p. 175.
5. A. J. Campillo and H-B. Lin, "Photothermal Spectroscopy of Aerosols," in *Photothermal Investigations of Solids and Fluids*, J. A. Sell, Ed. (Academic, New York, 1989), Chap. 10, p. 321.

6. J. D. Spear, R. E. Russo, and R. J. Silva, "Differential Photothermal Deflection Spectroscopy Using a Single Position Sensor," Appl. Spectrosc. **42**, 1103–1105 (1988).
7. R. Vyas, B. Monson, Y-X. Nie, and R. Gupta, "Continuous Wave Photothermal Deflection Spectroscopy in a Flowing Medium," Appl. Opt. **27**, 3914–3920 (1988).
8. A. Mandelis and B. S. H. Royce, "Fundamental-Mode Laser-Beam Propagation in Optically Inhomogeneous Electrochemical Media with Chemical Species Concentration Gradients," Appl. Opt. **23**, 2892–2901 (1984).
9. L. C. Aamodt and J. C. Murphy, "Photothermal Measurements Using a Localized Excitation Source," J. Appl. Phys. **52**, 4903–4914 (1981).
10. E. Legal Lasalle, F. Lepoutre, and J. P. Roger, "Probe Beam Size Effects in Photothermal Deflection Experiments," J. Appl. Phys. **64**, 1–5 (1988).
11. F. A. McDonald, G. C. Wetsel, Jr., and J. E. Jamieson, "Photothermal Beam-Deflection Imaging of Vertical Interfaces in Solids," Can. J. Phys. **64**, 1265–1268 (1986).
12. W. Nowacki, *Thermoelasticity* (Pergamon, New York, 1986).
13. Previous theoretical and experimental work has been published on $dn/\partial T$ in solids. A list of references can be found in R. M. Waxler, D. Horowitz, and A. Feldman, "Optical and Physical Parameters of Plexiglas 55 and Lexan," Appl. Opt. **18**, 101–104 (1979).
14. S. A. Akhmanov, R. V. Kokhlov, and A. P. Surhorukov, "Self-Focusing, Self-Defocusing and Self-Modulation of Laser Beams," in *Laser Handbook*, F. T. Arecchi and E. O. Schultz-Dubois, Eds. (North-Holland, Amsterdam, 1972), p. 1151.
15. *Smithsonian Physical Tables* (The Lord Baltimore Press, Baltimore, 1956).
16. *CRC Handbook of Chemistry and Physics* (Chemical Rubber Co., Cleveland, 1971).
17. N. J. Dovichi, T. G. Nolan, and W. A. Weiner, "Theory for Laser-Induced Photothermal Refraction," Anal. Chem. **56**, 1700–1704 (1984).
18. D. Solimini, "Loss Measurements of Organic Materials at 6328 Å," J. Appl. Phys. **37**, 3314–3315 (1966).
19. L. W. Tilton and J. K. Taylor, "Refractive Index and Dispersion of Distilled Water For Visible Radiation at Temperatures 0 to 60°C," J. Res. Natl. Bur. Stand. Sect. A **20**, 419–477 (1938). Values of dn/dT are derived from successive values of n at 1°C intervals, measured at the 656.28-nm spectral emission line of hydrogen.
20. J. C. Murphy and L. C. Aamodt, "Photothermal Spectroscopy Using Optical Beam Probing: Mirage Effect," J. Appl. Phys. **51**, 4580–4588 (1980).